Pseudo-Fourier modal analysis on dielectric slabs with arbitrary longitudinal permittivity and permeability profiles

Hwi Kim, Seyoon Kim, Il-Min Lee, and Byoungho Lee

School of Electrical Engineering, Seoul National University, Kwanak-Gu Shinlim-Dong, Seoul 151-744, Korea

Received December 9, 2005; accepted March 15, 2006; posted April 6, 2006 (Doc. ID 66505)

A pseudo-Fourier modal analysis method for analyzing finite-sized dielectric slabs with arbitrary longitudinal permittivity and permeability profiles is proposed. In the proposed method, the permittivity and permeability profiles are represented by the Fourier expansion without using the conventional staircase approximation. The total electromagnetic field distribution inside a dielectric slab is a linear superposition of extracted pseudo-Fourier eigenmodes with specific coupling coefficients selected to satisfy given boundary conditions. The proposed pseudo-Fourier modal analysis method shows excellent agreement with the conventional rigorous coupled-wave analysis with the S-matrix method. © 2006 Optical Society of America

OCIS codes: 050.0050, 050.1940, 050.1950, 050.1960, 260.1960.

1. INTRODUCTION

Many interesting optical structures such as layered diffraction gratings, photonic crystal slabs, and more general complex media[1] are commonly finite-sized dielectric slab structures with specific permittivity and permeability profiles. In analyzing dielectric slabs with arbitrary permittivity and permeability profiles, the modal analysis is a fundamental issue. In the modal analysis framework, the internal eigenmodes distinguished by their own characteristic eigenvalues are identified and their coupled dynamics are manifested. As a result, when an internal electromagnetic field distribution in a target structure is excited by an external source, the excited internal electromagnetic field distribution can be represented by a linear superposition of internal eigenmodes of the target structure. The coupling coefficient of an internal eigenmode in the linear superposition implies an important physical meaning.

For the past three decades, rigorous modal analysis methods on grating structures have been investigated persistently. Particularly, in cases of two-dimensional surface-relief gratings without a longitudinal permittivity variation along the direction (conventionally denoted by the z direction) normal to the grating surface, the rigorous coupled-wave analysis (RCWA)[2–5] is well established for modal analysis.

Carefully inspecting the coupled differential equation system in the framework of the classical RCWA, we can find that when longitudinal permittivity variation exists along the z direction, the formulation of the RCWA becomes a coupled linear second-order ordinary differential equation system with nonconstant coefficients, which cannot be handled with the conventional method. In this case, to escape from the difficulty, the RCWA takes up the S-matrix method that uses the staircase approximation[6–9] to represent the permittivity profile inside a dielectric slab. Therefore, for analyzing three-dimensional structures, the combination of the RCWA and the S-matrix method[6,7] is employed in general. The staircase approximation of the longitudinal permittivity profile is widely accepted in various grating analysis problems.

However, Popov *et al.*[9,10] analyzed the limitation and the validity of the staircase approximation in representing continuous grating profiles. They showed that the differential method without the staircase approximation gave more accurate results than the RCWA and the S-matrix method using the staircase approximation. Surely, the S-matrix method gives exact field distribution solutions for the staircase permittivity structures. The plane-wave expansion method (PWM) formulated by Sakoda[11,12] for analyzing reflection and transmission characteristics of finite-sized photonic crystals did not use the staircase approximation for modeling photonic crystals. But Sakoda's PWM showed poor convergence.

On the other hand, under the staircase approximation, only local eigenmodes in each interval with no permittivity variation along the z direction can be identified. In our viewpoint, the field representation under the staircase approximation cannot be truly modal analysis. An eigenmode must be identified by its specific eigenvalue. However, the field representation under the staircase approximation does not have such an eigenpair.

In this paper, a pseudo-Fourier modal analysis (PFMA) method without the staircase approximation is proposed for the rigorous modal analysis of finite-sized dielectric slabs with arbitrary permittivity and permeability profiles. In this paper, a prerequisite step that should be manifested before describing the fully generalized theory is addressed. Thus the proposed PFMA method is verified for one-dimensional structures. However, it is elucidated that the mathematical technique for one-dimensional structures introduced in this paper will be straightforwardly extended to three-dimensional structure analysis. The fully generalized theory will be completed in a future paper.

This paper is organized as follows. In Section 2 continuous representation of permittivity and permeability profiles in the RCWA scheme is accounted for. In Section 3 the convergence of the pseudo-Fourier representation of the electromagnetic field is discussed and the main eigenvalue equation is formulated. In Section 4 the identification and extraction of the eigenmodes and eigenvalues are described based on the results of Section 3. In Section 5 the boundary conditions are discussed and the total field distributions in finite-sized slabs are analyzed. The total field distributions obtained by the proposed method are compared with those obtained by the S-matrix method. In Section 6 concluding remarks and the perspective on the generalization of the proposed method to slab structures with finite thickness and three-dimensional arbitrary permittivity and permeability profiles are given.

2. CONTINUOUS FOURIER REPRESENTATION OF PERMITTIVITY AND PERMEABILITY PROFILES IN THE RIGOROUS COUPLED-WAVE ANALYSIS SCHEME

The coupled linear differential equation system of the classical RCWA is reviewed. In the description of the theory, vectors are underlined and matrices are underlined twice. In the classical RCWA scheme, the internal electric and magnetic field distributions inside a grating are expressed, respectively, as the following symmetrically truncated Bloch mode expansions:

$$\underline{E}(x,y,z) = \sum_{m=-M}^{M} \sum_{n=-N}^{N} [S_{x,mn}(z)\underline{x} + S_{y,mn}(z)\underline{y} + S_{z,mn}(z)\underline{z}]\exp[j(k_{x,m}x + k_{y,n}y)], \tag{1a}$$

$$\underline{H}(x,y,z) = j\sqrt{\frac{\varepsilon_0}{\mu_0}} \sum_{m=-M}^{M} \sum_{n=-N}^{N} [U_{x,mn}(z)\underline{x} + U_{y,mn}(z)\underline{y} + U_{z,mn}(z)\underline{z}]\exp[j(k_{x,m}x + k_{y,n}y)], \tag{1b}$$

where $k_{x,m}$ and $k_{y,n}$ are the mth x-direction wave-vector component and the nth y-direction wave-vector component, respectively. They are given, respectively, by

$$k_{x,m} = k_x + mG_x \quad \text{for } -M \le m \le M, \tag{2a}$$

$$k_{y,n} = k_y + nG_y \quad \text{for } (-N \le n \le N), \tag{2b}$$

where G_x and G_y are the x- and y-direction grating vectors, respectively. We substitute the field representations in Eqs. (1a) and (1b) into the following Maxwell equations,

$$\nabla \times \underline{E} = j\omega\mu_0\mu(x,y,z)(H_x\underline{x} + H_y\underline{y} + H_z\underline{z}), \tag{3a}$$

$$\nabla \times \underline{H} = -j\omega\varepsilon_0\varepsilon(x,y,z)(E_x\underline{x} + E_y\underline{y} + E_z\underline{z}), \tag{3b}$$

where ε_0 and μ_0 are electric permittivity and magnetic permeability in free space, and the permittivity profile $\varepsilon(x,y,z)$ and the permeability profile $\mu(x,y,z)$ take the Fourier series forms, respectively, as

$$\varepsilon(x,y,z) = \sum_{m=-2M}^{2M} \sum_{n=-2N}^{2N} \tilde{\varepsilon}_{m,n}(z)\exp[j(mG_x x + nG_y y)], \tag{4a}$$

$$\mu(x,y,z) = \sum_{m=-2M}^{2M} \sum_{n=-2N}^{2N} \tilde{\mu}_{m,n}(z)\exp[j(mG_x x + nG_y y)]. \tag{4b}$$

Then the following coupled linear differential equation systems are obtained:

$$\frac{dS_{y,mn}(z)}{dz} = k_0\sum_{s,t} \tilde{\mu}_{m-s,n-t}(z)U_{x,st}(z) + jk_{y,n}S_{z,mn}(z), \tag{5a}$$

$$\frac{dS_{x,mn}(z)}{dz} = -k_0\sum_{s,t} \tilde{\mu}_{m-s,n-t}(z)U_{y,st}(z) + jk_{x,m}S_{z,mn}(z), \tag{5b}$$

$$\sum_{s,t} \tilde{\varepsilon}_{m-s,n-t}(z)S_{z,s,t}(z) = \frac{-j}{k_0}[k_{x,m}U_{y,mn}(z) - k_{y,n}U_{x,mn}(z)], \tag{5c}$$

$$\frac{dU_{y,mn}(z)}{dz} = jk_{y,n}U_{z,mn}(z) + k_0\sum_{s,t} \tilde{\varepsilon}_{m-s,n-t}(z)S_{x,st}(z), \tag{5d}$$

$$\frac{dU_{x,mn}(z)}{dz} = -k_0\sum_{s,t} \varepsilon_{m-s,n-t}(z)S_{y,s,t}(z) + jk_{x,m}U_{z,mn}(z), \tag{5e}$$

$$\sum_{s,t} \tilde{\mu}_{m-s,n-t}(z)U_{z,mn}(z) = \frac{-j}{k_0}[k_{x,m}S_{y,mn}(z) - k_{y,n}S_{x,mn}(z)]. \tag{5f}$$

The coefficients in Eqs. (5a)–(5f) are functions of the variable z. As mentioned previously, the staircase approximation of $\varepsilon(x,y,z)$ and $\mu(x,y,z)$ along the z axis enables the coupled equation system to be approximated to the equation system with constant coefficients in each staircase interval. The S-matrix method is a recursive matrix algorithm used to match the boundary conditions at all boundaries generated by the staircase approximation.

In this paper, we propose an analysis method for solving Eqs. (5a)–(5f) without the staircase approximation. To reveal the main concept of the proposed method, it is enough to consider the cases of longitudinal one-dimensional structures. The permittivity and permeability profiles of a longitudinal one-dimensional structure are given by $\varepsilon(z)$ and $\mu(z)$, respectively. In this case the coupled differential equation system of Eqs. (5a)–(5f) becomes simplified but the coefficients are z-dependent functions.

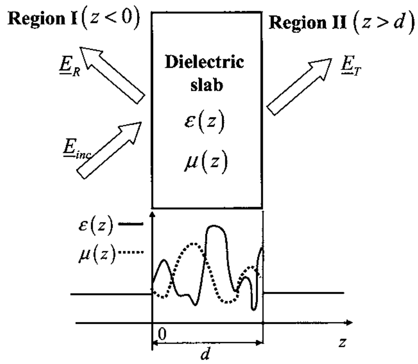

Fig. 1. Dielectric slab with arbitrary one-dimensional permittivity and permeability profiles.

3. PSEUDO-FOURIER REPRESENTATION OF EIGENMODES AND EIGENVALUE EQUATION

In the case of a one-dimensional structure, the dielectric structure is a slab with longitudinal permittivity and permeability profiles as shown in Fig. 1. Figure 1 shows a dielectric slab of finite thickness d with arbitrary permittivity profile $\varepsilon(z)$ and permeability profile $\mu(z)$ placed between region I and region II. In this paper, both the permittivity $\varepsilon(z)$ and the permeability $\mu(z)$ are assumed to satisfy the following relations:

1. $\varepsilon(z)>0$ and $\mu(z)>0$, which mean that the slab structure is made of dielectric material.
2. $\varepsilon(z)$ and $\mu(z)$ are piecewise-continuous functions bounded in the range of $0\le z\le d$.

Let an incident wave $\underline{E}_{\text{inc}}$ impinge from region I to the dielectric slab. The incident wave is assumed to be a plane wave with an incidence angle of θ, an azimuthal angle of ϕ, and a polarization angle of ψ with free-space wavelength λ. The incident wave is represented as

$$\underline{E}_{\text{inc}} = (U_x\underline{x} + U_y\underline{y} + U_z\underline{z})\exp[j(k_{\text{I},x}x + k_{\text{I},y}y + k_{\text{I},z}z)], \tag{6a}$$

where U_x, U_y, and U_z are given by

$$(U_x,U_y,U_z) = (\cos\psi\cos\theta\cos\phi - \sin\psi\sin\phi, \cos\psi\cos\theta\sin\phi + \sin\psi\cos\phi, -\cos\psi\sin\theta), \tag{6b}$$

and $k_{\text{I},x}$, $k_{\text{I},y}$, and $k_{\text{I},z}$ are given by

$$(k_{\text{I},x},k_{\text{I},y},k_{\text{I},z}) = (k_0 n_{\text{I}}\sin\theta\cos\phi, k_0 n_{\text{I}}\sin\theta\sin\phi, k_0 n_{\text{I}}\cos\theta), \tag{6c}$$

with $k_0=2\pi/\lambda$ and n_{I} is the refractive index of region I. The reflected and transmitted waves in regions I and II are represented, respectively, as

$$\underline{E}_{\text{I}} = \underline{E}_{\text{inc}} + (R_x\underline{x} + R_y\underline{y} + R_z\underline{z})\exp[j(k_{\text{I},x}x + k_{\text{I},y}y - k_{\text{I},z}z)], \tag{7a}$$

$$\underline{E}_{\text{II}} = (T_x\underline{x} + T_y\underline{y} + T_z\underline{z})\exp[j(k_{\text{II},x}x + k_{\text{II},y}y + k_{\text{II},z}(z-d))], \tag{7b}$$

where R_x, R_y, R_z are reflected wave components and T_x, T_y, T_z are the transmitted wave components. To satisfy the phase-matching conditions on the transverse plane ($z=0$ and $z=d$), the wave-vector components hold the following relations:

$$k_{\text{I},x} = k_{\text{II},x} = k_0 n_{\text{I}}\sin\theta\cos\phi, \tag{8a}$$

$$k_{\text{I},y} = k_{\text{II},y} = k_0 n_{\text{I}}\sin\theta\sin\phi, \tag{8b}$$

$$k_{\text{I},z} = k_0 n_{\text{I}}\cos\theta, \tag{8c}$$

$$k_{\text{II},z} = (k_0^2 n_{\text{II}}^2 - k_0^2 n_{\text{I}}^2\sin^2\theta)^{1/2}, \tag{8d}$$

where $(k_{\text{II},x},k_{\text{II},y},k_{\text{II},z})$ is the wave vector in region II, and n_{II} is the refractive index of region II.

The internal electric and magnetic field distributions inside the slab structure are given, from Eqs. (1a) and (1b), as

$$\underline{E}(x,y,z) = [S_x(z)\underline{x} + S_y(z)\underline{y} + S_z(z)\underline{z}] \times \exp[j(k_x x + k_y y)], \tag{9a}$$

$$\underline{H}(x,y,z) = j\sqrt{\varepsilon_0/\mu_0}[U_x(z)\underline{x} + U_y(z)\underline{y} + U_z(z)\underline{z}] \times \exp[j(k_x x + k_y y)]. \tag{9b}$$

Then the pseudo-Fourier representation of eigenmodes in a dielectric slab is described. At first, the periodic extensions of the permittivity profile $\varepsilon(z)$ and the permeability profile $\mu(z)$, $\hat{\varepsilon}(z)$ and $\hat{\mu}(z)$, are defined, respectively, as

$$\hat{\varepsilon}(z) = \varepsilon(z) \otimes \sum_{n=-\infty}^{+\infty}\delta(z-nd), \tag{10a}$$

$$\hat{\mu}(z) = \mu(z) \otimes \sum_{n=-\infty}^{+\infty}\delta(z-nd), \tag{10b}$$

where $\otimes$ denotes convolution. Figure 2 shows the periodic extension $\hat{\varepsilon}(z)$ of a permittivity profile $\varepsilon(z)$ with a fundamental period of d. In the periodic extension of the dielectric slab with $\hat{\varepsilon}(z)$ and $\hat{\mu}(z)$, any existing internal electromagnetic field can be represented by a linear superposition of the pseudo-Fourier eigenmodes of the periodic extension from the Bloch theorem.[12,13]

From the Bloch theorem, the pseudo-Fourier eigenmodes of the electric and magnetic fields inside the periodic extension of the dielectric slab are given, respectively, by

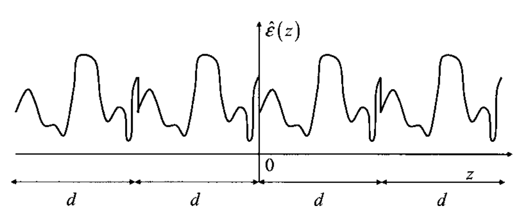

Fig. 2. Periodic extension of a finite-sized dielectric slab with one-dimensional arbitrary permittivity profile.

$$\underline{E}_{\underline{k}}(z) = \exp[j(k_x x + k_y y + k_z z)]\underline{\hat{E}}_{\underline{k}}(z), \tag{11a}$$

$$\underline{H}_{\underline{k}}(z) = \exp[j(k_x x + k_y y + k_z z)]\underline{\hat{H}}_{\underline{k}}(z), \tag{11b}$$

where $\underline{k}$ denotes the wave vector (k_x, k_y, k_z). Here k_z is considered as the eigenvalue of the pseudo-Fourier eigenmode $(\underline{E}_{\underline{k}}(z), \underline{H}_{\underline{k}}(z))$. Since both $\underline{\hat{E}}_{\underline{k}}(z)$ and $\underline{\hat{H}}_{\underline{k}}(z)$ are periodic functions with a fundamental period d, they can be approximately expressed by truncated Fourier series.

We introduce the asymmetrically truncated Fourier representations of $\underline{\hat{E}}_{\underline{k}}(z)$ and $\underline{\hat{H}}_{\underline{k}}(z)$. The asymmetrically truncated Fourier representations of $\underline{\hat{E}}_{\underline{k}}(z)$ and $\underline{\hat{H}}_{\underline{k}}(z)$ with $2N+1$ harmonic components, $\underline{\hat{E}}_{\underline{k}}^{(N,m)}(z)$ and $\underline{\hat{H}}_{\underline{k}}^{(N,m)}(z)$, are expressed as

$$\underline{\hat{E}}_{\underline{k}}^{(N,m)}(z) = \sum_{p=-N+m}^{N+m} (\tilde{E}_{x,p}\underline{x} + \tilde{E}_{y,p}\underline{y} + \tilde{E}_{z,p}\underline{z})\exp(jpG_z z), \tag{12a}$$

$$\underline{\hat{H}}_{\underline{k}}^{(N,m)}(z) = j\sqrt{\frac{\varepsilon_0}{\mu_0}} \sum_{p=-N+m}^{N+m} (\tilde{H}_{x,p}\underline{x} + \tilde{H}_{y,p}\underline{y} + \tilde{H}_{z,p}\underline{z})\exp(jpG_z z), \tag{12b}$$

where m is an integer in the range $-N \le m \le N$, the reciprocal vector G_z is given by $2\pi/d$, and the number of the asymmetrically truncated Fourier representations of a pseudo-Fourier eigenmode is just $2N+1$ (see Appendix A). By substituting Eqs. (12a) and (12b) into Eqs. (11a) and (11b), the pseudo-Fourier eigenmode $(\underline{E}_{\underline{k}}(z), \underline{H}_{\underline{k}}(z))$ for a wave vector $\underline{k}$ is expressed by $2N+1$ asymmetrically truncated pseudo-Fourier representations as follows:

$$\underline{E}_{\underline{k}}^{(N,m)}(z) = \exp[j(k_x x + k_y y)] \sum_{p=-N+m}^{N+m} (\tilde{E}_{x,p}\underline{x} + \tilde{E}_{y,p}\underline{y} + \tilde{E}_{z,p}\underline{z}) \times \exp[j(pG_z + k_z^{(N,m)})z], \tag{13a}$$

$$\underline{H}_{\underline{k}}^{(N,m)}(z) = \exp[j(k_x x + k_y y)] j\sqrt{\frac{\varepsilon_0}{\mu_0}} \sum_{p=-N+m}^{N+m} (\tilde{H}_{x,p}\underline{x} + \tilde{H}_{y,p}\underline{y} + \tilde{H}_{z,p}\underline{z})\exp[j(pG_z + k_z^{(N,m)})z], \tag{13b}$$

where $k_z^{(N,m)}$ is an approximate value of k_z in the asymmetrically truncated pseudo-Fourier representation. According to the analysis on the uniform convergence of the Fourier representation established by Li,[14] we can see that there exists a nonnegative integer pair $(N^*, m^*(N))$ satisfying the inequalities, i.e., the convergence criteria;

$$|\underline{E}_{\underline{k}}(z) - \underline{E}_{\underline{k}}^{(N,m)}(z)| < \sigma_E, \quad |\underline{H}_{\underline{k}}(z) - \underline{H}_{\underline{k}}^{(N,m)}(z)| < \sigma_H,$$

$$|k_z - k_z^{(N,m)}| < \sigma_k, \tag{14}$$

where $N \ge N^*$ and $|m| \le m^*(N) \le N$ is satisfied for small positive real numbers σ_E, σ_H, and σ_k, and k_z is a true eigenvalue of the true pseudo-Fourier eigenmode $(\underline{E}_{\underline{k}}(z), \underline{H}_{\underline{k}}(z))$. Additionally assuming that the envelop profile of the pseudo-Fourier mode $[\underline{\hat{E}}_{\underline{k}}(z), \underline{\hat{H}}_{\underline{k}}(z)]$ is nearly band limited, we can confirm that there definitely exist finite positive integers N^* and $m^*(N)$.

According to the convergence criteria of inequalities (14), the asymmetrically truncated Fourier representations of a pseudo-Fourier eigenmode, Eqs. (13a) and (13b), can be classified into three classes as indicated in Fig. 3. Figure 3 shows the discrete distribution of the Fourier coefficient $\tilde{E}_{x,p}$ (or $\tilde{E}_{y,p}$) in the Fourier space. The first class [denoted by (i) in Fig. 3(a)] indicates that the total number of used harmonics, $2N+1$, is larger than the lower bound $2N^*+1$, but the shift index m is outside the convergence range $[-m^*, m^*]$. The third class [denoted by (iii) in Fig. 3(b)] shows the deficiency of harmonic components used in the pseudo-Fourier representation. But the second class [denoted by (ii) in Fig. 3(a)] satisfies the convergence criterion of inequalities (14). It is expected that with enough harmonic components in the pseudo-Fourier representation, a few in class (iii) having a large shift index m satisfying $|m| > m^*$ are considerably different from the others included in class (ii). Also, it is expected that the representations belonging to class (ii) would produce an almost similar field profile and almost the same eigenvalue $k_z^{(N,m)}$ according to the convergence criterion of inequalities (14). This point will be definitely manifested through numerical simulations in Section 4.

Conclusively, we can see that classes (i) and (iii) cannot correctly represent the true pseudo-Fourier eigenmode because of significant loss of nonzero high-frequency harmonic components, while class (ii) correctly expresses the true pseudo-Fourier eigenmode. In addition, the total number of Fourier representations precisely describing the true solution [that is, satisfying the convergence criterion of inequalities (14) and belonging to class (ii)] is $2m^*(N)+1$. The other $2(N-m^*(N))$ representations do not satisfy the convergence criteria of inequalities (14).

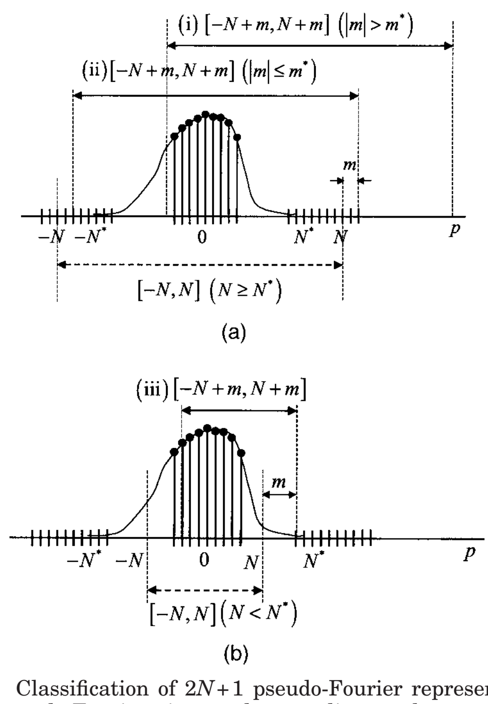

Fig. 3. Classification of $2N+1$ pseudo-Fourier representations of the pseudo-Fourier eigenmode according to the convergence condition.

On the other hand, the pseudo-Fourier eigenmodes, Eqs. (13a) and (13b), must satisfy the following Maxwell equations:

$$\nabla \times \underline{E} = j\omega\mu_0\hat{\mu}(z)(H_x\underline{x} + H_y\underline{y} + H_z\underline{z}), \tag{15a}$$

$$\nabla \times \underline{H} = -j\omega\varepsilon_0\hat{\varepsilon}(z)(E_x\underline{x} + E_y\underline{y} + E_z\underline{z}), \tag{15b}$$

where the periodic extensions of the permittivity and the permeability profiles $\hat{\varepsilon}(z)$ and $\hat{\mu}(z)$ take the Fourier series form as

$$\hat{\varepsilon}(z) = \sum_{g=-2N}^{2N} \tilde{\varepsilon}_g \exp(jG_z gz), \tag{16a}$$

$$\hat{\mu}(z) = \sum_{g=-2N}^{2N} \tilde{\mu}_g \exp(jG_z gz). \tag{16b}$$

Let $k_z^{(N,m)}+pG_z$ denoted by $k_{z,p}$ as $k_{z,p}=k_z^{(N,m)}+pG_z$; then by substituting the pseudo-Fourier representations of Eqs. (13a) and (13b) into Maxwell's Eqs. (15a) and (15b), Maxwell's equations are translated into the algebraic equation system of the Fourier coefficients of Eqs. (13a) and (13b) as

$$jk_{z,p}\tilde{E}_{y,p} = k_0 \sum_{s=-N+m}^{N+m} \tilde{\mu}_{p-s}\tilde{H}_{x,s} + jk_y\tilde{E}_{z,p}, \tag{17a}$$

$$jk_{z,p}\tilde{E}_{x,p} = -k_0 \sum_{s=-N+m}^{N+m} \tilde{\mu}_{p-s}\tilde{H}_{y,s} + jk_x\tilde{E}_{z,p}, \tag{17b}$$

$$\sum_{s=-N+m}^{N+m} \tilde{\varepsilon}_{p-s}\tilde{E}_{z,s} = -\frac{jk_x}{k_0}\tilde{H}_{y,p} + \frac{jk_y}{k_0}\tilde{H}_{x,p}, \tag{17c}$$

$$\frac{jk_{z,p}}{k_0}\tilde{H}_{y,p} = \sum_{s=-N+m}^{N+m} \tilde{\varepsilon}_{p-s}\tilde{E}_{x,s} + \frac{jk_y}{k_0}\tilde{H}_{z,p}, \tag{17d}$$

$$\frac{jk_{z,p}}{k_0}\tilde{H}_{x,p} = -\sum_{s=-N+m}^{N+m} \tilde{\varepsilon}_{p-s}\tilde{E}_{y,s} + \frac{jk_x}{k_0}\tilde{H}_{z,p}, \tag{17e}$$

$$\sum_{s=-N+m}^{N+m} \tilde{\mu}_{p-s}\tilde{H}_{z,s} = \frac{-jk_x}{k_0}\tilde{E}_{y,p} + \frac{jk_y}{k_0}\tilde{E}_{x,p}, \tag{17f}$$

where the integer indices s and p are in the range of $-N+m \le s$ and $p \le N+m$. The algebraic equation system of Eqs. (17a)–(17f) can be manipulated as a matrix form. For this, the following notations are adopted.

The Toeplitz matrices $\underline{\underline{\varepsilon}}$ of $\tilde{\varepsilon}_g$ and $\underline{\underline{\mu}}$ of $\tilde{\mu}_g$ are defined, respectively, as

$$\underline{\underline{\varepsilon}} = \begin{bmatrix} \tilde{\varepsilon}_0 & \tilde{\varepsilon}_{-1} & \cdots & \tilde{\varepsilon}_{-2N} \\ \tilde{\varepsilon}_1 & \tilde{\varepsilon}_0 & & \tilde{\varepsilon}_{-2N+1} \\ \vdots & \vdots & & \\ \tilde{\varepsilon}_{2N} & \tilde{\varepsilon}_{2N-1} & \cdots & \tilde{\varepsilon}_0 \end{bmatrix}, \tag{18a}$$

$$\underline{\underline{\mu}} = \begin{bmatrix} \tilde{\mu}_0 & \tilde{\mu}_{-1} & \cdots & \tilde{\mu}_{-2N} \\ \tilde{\mu}_1 & \tilde{\mu}_0 & & \tilde{\mu}_{-2N+1} \\ \vdots & \vdots & & \\ \tilde{\mu}_{2N} & \tilde{\mu}_{2N-1} & \cdots & \tilde{\mu}_0 \end{bmatrix}. \tag{18b}$$

$\underline{\underline{G}}_z|_{-N+m}^{N+m}$, $\underline{\underline{K}}_z|_{-N+m}^{N+m}$, $\underline{\underline{K}}_y$, and $\underline{\underline{K}}_x$ are defined, respectively, as

$$\underline{\underline{G}}_z|_{-N+m}^{N+m} = \begin{bmatrix} \frac{(-N+m)G_z}{k_0} & 0 & \cdots & 0 \\ 0 & \frac{(-N+m+1)G_z}{k_0} & 0 & 0 \\ \vdots & \vdots & \ddots & 0 \\ 0 & 0 & \cdots & \frac{(N+m)G_z}{k_0} \end{bmatrix}, \tag{18c}$$

$$\underline{\underline{K}}_z|_{-N+m}^{N+m} = (k_z^{(N,m)}/k_0)\underline{\underline{I}} + \underline{\underline{G}}_z|_{-N+m}^{N+m}, \tag{18d}$$

$$\underline{\underline{K}}_y = (k_y/k_0)\underline{\underline{I}}, \tag{18e}$$

$$\underline{\underline{K}}_x = (k_x/k_0)\underline{\underline{I}}, \tag{18f}$$

where $\underline{\underline{I}}$ is the $(2N+1)\times(2N+1)$ identity matrix. The vector notations $\underline{\tilde{E}}_x|_{-N+m}^{N+m}$, $\underline{\tilde{E}}_y|_{-N+m}^{N+m}$, $\underline{\tilde{H}}_x|_{-N+m}^{N+m}$, and $\underline{\tilde{H}}_y|_{-N+m}^{N+m}$ are defined, respectively, as

$$\underline{\tilde{E}}_y|_{-N+m}^{N+m} = [\tilde{E}_{y,-N+m} \quad \tilde{E}_{y,-N+m+1} \quad \cdots \quad \tilde{E}_{y,N+m}]^t, \tag{19a}$$

$$\underline{\tilde{E}}_x|_{-N+m}^{N+m} = [\tilde{E}_{x,-N+m} \quad \tilde{E}_{x,-N+m+1} \quad \cdots \quad \tilde{E}_{x,N+m}]^t, \tag{19b}$$

$$\underline{\tilde{H}}_x\Big|_{-N+m}^{N+m} = [\tilde{H}_{x,-N+m} \quad \tilde{H}_{x,-N+m+1} \quad \cdots \quad \tilde{H}_{x,N+m}]^t, \tag{19c}$$

$$\underline{\tilde{H}}_y\Big|_{-N+m}^{N+m} = [\tilde{H}_{y,-N+m} \quad \tilde{H}_{y,-N+m+1} \quad \cdots \quad \tilde{H}_{y,N+m}]^t. \tag{19d}$$

Then, with use of the above notations, the algebraic equation system of Eqs. (17a)–(17f) is rewritten as

$$j\underline{\underline{K}}_z\Big|_{-N+m}^{N+m}\underline{\tilde{E}}_y\Big|_{-N+m}^{N+m} = \underline{\underline{\mu}}\underline{\tilde{H}}_x\Big|_{-N+m}^{N+m} + j\underline{\underline{K}}_y\underline{\tilde{E}}_z\Big|_{-N+m}^{N+m}, \tag{20a}$$

$$j\underline{\underline{K}}_z\Big|_{-N+m}^{N+m}\underline{\tilde{E}}_x\Big|_{-N+m}^{N+m} = -\underline{\underline{\mu}}\underline{\tilde{H}}_y\Big|_{-N+m}^{N+m} + j\underline{\underline{K}}_x\underline{\tilde{E}}_z\Big|_{-N+m}^{N+m}, \tag{20b}$$

$$\underline{\underline{\varepsilon}}\underline{\tilde{E}}_z\Big|_{-N+m}^{N+m} = -j\underline{\underline{K}}_x\underline{\tilde{H}}_y\Big|_{-N+m}^{N+m} + j\underline{\underline{K}}_y\underline{\tilde{H}}_x\Big|_{-N+m}^{N+m}, \tag{20c}$$

$$j\underline{\underline{K}}_z\Big|_{-N+m}^{N+m}\underline{\tilde{H}}_y\Big|_{-N+m}^{N+m} = j\underline{\underline{K}}_y\underline{\tilde{H}}_z\Big|_{-N+m}^{N+m} + \underline{\underline{\varepsilon}}\underline{\tilde{E}}_x\Big|_{-N+m}^{N+m}, \tag{20d}$$

$$j\underline{\underline{K}}_z\Big|_{-N+m}^{N+m}\underline{\tilde{H}}_x\Big|_{-N+m}^{N+m} = -\underline{\underline{\varepsilon}}\underline{\tilde{E}}_y\Big|_{-N+m}^{N+m} + j\underline{\underline{K}}_x\underline{\tilde{H}}_z\Big|_{-N+m}^{N+m}, \tag{20e}$$

$$\underline{\underline{\mu}}\underline{\tilde{H}}_z\Big|_{-N+m}^{N+m} = -j\underline{\underline{K}}_x\underline{\tilde{E}}_y\Big|_{-N+m}^{N+m} + j\underline{\underline{K}}_y\underline{\tilde{E}}_x\Big|_{-N+m}^{N+m}. \tag{20f}$$

The algebraic equation system of Eqs. (20a)–(20f) is considered as the following matrix eigenvalue equation of $(8N+4)\times(8N+4)$ dimensions:

$$\begin{bmatrix} -j\underline{\underline{G}}_z\Big|_{-N+m}^{N+m} & 0 & \underline{\underline{K}}_y\underline{\underline{\varepsilon}}^{-1}\underline{\underline{K}}_x & \underline{\underline{\mu}} - \underline{\underline{K}}_y\underline{\underline{\varepsilon}}^{-1}\underline{\underline{K}}_y \\ 0 & -j\underline{\underline{G}}_z\Big|_{-N+m}^{N+m} & -\underline{\underline{\mu}} + \underline{\underline{K}}_x\underline{\underline{\varepsilon}}^{-1}\underline{\underline{K}}_x & -\underline{\underline{K}}_x\underline{\underline{\varepsilon}}^{-1}\underline{\underline{K}}_y \\ \underline{\underline{K}}_y\underline{\underline{\mu}}^{-1}\underline{\underline{K}}_x & \underline{\underline{\varepsilon}} - \underline{\underline{K}}_y\underline{\underline{\mu}}^{-1}\underline{\underline{K}}_y & -j\underline{\underline{G}}_z\Big|_{-N+m}^{N+m} & 0 \\ -\underline{\underline{\varepsilon}} + \underline{\underline{K}}_x\underline{\underline{\mu}}^{-1}\underline{\underline{K}}_x & -\underline{\underline{K}}_x\underline{\underline{\mu}}^{-1}\underline{\underline{K}}_y & 0 & -j\underline{\underline{G}}_z\Big|_{-N+m}^{N+m} \end{bmatrix} \begin{pmatrix} \underline{\tilde{E}}_y\Big|_{-N+m}^{N+m} \\ \underline{\tilde{E}}_x\Big|_{-N+m}^{N+m} \\ \underline{\tilde{H}}_y\Big|_{-N+m}^{N+m} \\ \underline{\tilde{H}}_x\Big|_{-N+m}^{N+m} \end{pmatrix} = j\frac{k_z^{(N,m)}}{k_0} \begin{pmatrix} \underline{\tilde{E}}_y\Big|_{-N+m}^{N+m} \\ \underline{\tilde{E}}_x\Big|_{-N+m}^{N+m} \\ \underline{\tilde{H}}_y\Big|_{-N+m}^{N+m} \\ \underline{\tilde{H}}_x\Big|_{-N+m}^{N+m} \end{pmatrix}. \tag{21}$$

The reciprocal permittivity profile $\hat{\alpha}(z)$ and the reciprocal permeability $\hat{\beta}(z)$ are defined, respectively, as

$$\hat{\alpha}(z) = \frac{1}{\hat{\varepsilon}(z)} = \sum_{g=-2N}^{2N} \tilde{\alpha}_g \exp(jG_z g x), \tag{22a}$$

$$\hat{\beta}(z) = \frac{1}{\hat{\mu}(z)} = \sum_{g=-2N}^{2N} \tilde{\beta}_g \exp(jG_z g x). \tag{22b}$$

Then their Toeplitz matrices $\underline{\underline{\alpha}}$ and $\underline{\underline{\beta}}$ are taken, respectively, as

$$\underline{\underline{\alpha}} = \begin{bmatrix} \tilde{\alpha}_0 & \tilde{\alpha}_{-1} & \cdots & \tilde{\alpha}_{-2N} \\ \tilde{\alpha}_1 & \tilde{\alpha}_0 & & \tilde{\alpha}_{-2N+1} \\ \vdots & \vdots & & \\ \tilde{\alpha}_{2N} & \tilde{\alpha}_{2N-1} & \cdots & \tilde{\alpha}_0 \end{bmatrix}, \tag{23a}$$

$$\underline{\underline{\beta}} = \begin{bmatrix} \tilde{\beta}_0 & \tilde{\beta}_{-1} & \cdots & \tilde{\beta}_{-2N} \\ \tilde{\beta}_1 & \tilde{\beta}_0 & & \tilde{\beta}_{-2N+1} \\ \vdots & \vdots & & \\ \tilde{\beta}_{2N} & \tilde{\beta}_{2N-1} & \cdots & \tilde{\beta}_0 \end{bmatrix}. \tag{23b}$$

According to Lalanne and Morris's and Li's previous works on the convergence of the Fourier representation,[3,14] $\underline{\underline{\alpha}}$ is substituted into $\underline{\underline{\varepsilon}}^{-1}$ in Eq. (21) to obtain the stable convergence of the pseudo-Fourier representation. Thus, the main eigenvalue equation reads as

$$\begin{bmatrix} -j\underline{\underline{G}}_z\Big|_{-N+m}^{N+m} & 0 & \underline{\underline{K}}_y\underline{\underline{\alpha}}\underline{\underline{K}}_x & \underline{\underline{\mu}} - \underline{\underline{K}}_y\underline{\underline{\alpha}}\underline{\underline{K}}_y \\ 0 & -j\underline{\underline{G}}_z\Big|_{-N+m}^{N+m} & -\underline{\underline{\mu}} + \underline{\underline{K}}_x\underline{\underline{\alpha}}\underline{\underline{K}}_x & -\underline{\underline{K}}_x\underline{\underline{\alpha}}\underline{\underline{K}}_y \\ \underline{\underline{K}}_y\underline{\underline{\beta}}\underline{\underline{K}}_x & \underline{\underline{\varepsilon}} - \underline{\underline{K}}_y\underline{\underline{\beta}}\underline{\underline{K}}_y & -j\underline{\underline{G}}_z\Big|_{-N+m}^{N+m} & 0 \\ -\underline{\underline{\varepsilon}} + \underline{\underline{K}}_x\underline{\underline{\beta}}\underline{\underline{K}}_x & -\underline{\underline{K}}_x\underline{\underline{\beta}}\underline{\underline{K}}_y & 0 & -j\underline{\underline{G}}_z\Big|_{-N+m}^{N+m} \end{bmatrix} \begin{pmatrix} \underline{\tilde{E}}_y\Big|_{-N+m}^{N+m} \\ \underline{\tilde{E}}_x\Big|_{-N+m}^{N+m} \\ \underline{\tilde{H}}_y\Big|_{-N+m}^{N+m} \\ \underline{\tilde{H}}_x\Big|_{-N+m}^{N+m} \end{pmatrix} = j\frac{k_z^{(N,m)}}{k_0} \begin{pmatrix} \underline{\tilde{E}}_y\Big|_{-N+m}^{N+m} \\ \underline{\tilde{E}}_x\Big|_{-N+m}^{N+m} \\ \underline{\tilde{H}}_y\Big|_{-N+m}^{N+m} \\ \underline{\tilde{H}}_x\Big|_{-N+m}^{N+m} \end{pmatrix}. \tag{24}$$

Here, $k_z^{(N,m)}$ and $[\underline{\tilde{E}}_y|_{-N+m}^{N+m} \quad \underline{\tilde{E}}_x|_{-N+m}^{N+m} \quad \underline{\tilde{H}}_y|_{-N+m}^{N+m} \quad \underline{\tilde{H}}_x|_{-N+m}^{N+m}]^t$ are identified as an eigenvalue and an eigenvector, respectively. Considering Eqs. (13a) and (13b), we can see that the eigenvector $[\underline{\tilde{E}}_y|_{-N+m}^{N+m} \quad \underline{\tilde{E}}_x|_{-N+m}^{N+m} \quad \underline{\tilde{H}}_y|_{-N+m}^{N+m} \quad \underline{\tilde{H}}_x|_{-N+m}^{N+m}]^t$ corresponds to a pseudo-Fourier eigenmode, $(\underline{E}_k^{(N,m)}(z), \underline{H}_k^{(N,m)}(z))$, which can be distinguished by its own eigenvalue denoted by $k_z^{(N,m)}$.

On the other hand, from Eq. (18c), the matrix Eq. (24) is arranged as

$$
\begin{bmatrix}
-j\underline{\underline{G}}_z\big|_{-N}^{N} & 0 & \underline{\underline{K}}_y\underline{\underline{\alpha}}\underline{\underline{K}}_x & \underline{\underline{\mu}}-\underline{\underline{K}}_y\underline{\underline{\alpha}}\underline{\underline{K}}_y \\
0 & -j\underline{\underline{G}}_z\big|_{-N}^{N} & -\underline{\underline{\mu}}+\underline{\underline{K}}_x\underline{\underline{\alpha}}\underline{\underline{K}}_x & -\underline{\underline{K}}_x\underline{\underline{\alpha}}\underline{\underline{K}}_y \\
\underline{\underline{K}}_y\underline{\underline{\beta}}\underline{\underline{K}}_x & \underline{\underline{\varepsilon}}-\underline{\underline{K}}_y\underline{\underline{\beta}}\underline{\underline{K}}_y & -j\underline{\underline{G}}_z\big|_{-N}^{N} & 0 \\
-\underline{\underline{\varepsilon}}+\underline{\underline{K}}_x\underline{\underline{\beta}}\underline{\underline{K}}_x & -\underline{\underline{K}}_x\underline{\underline{\beta}}\underline{\underline{K}}_y & 0 & -j\underline{\underline{G}}_z\big|_{-N}^{N}
\end{bmatrix}
\times\begin{pmatrix}
\underline{\tilde{E}}_y\big|_{-N+m}^{N+m} \\
\underline{\tilde{E}}_x\big|_{-N+m}^{N+m} \\
\underline{\tilde{H}}_y\big|_{-N+m}^{N+m} \\
\underline{\tilde{H}}_x\big|_{-N+m}^{N+m}
\end{pmatrix}
= j\left(\frac{k_z^{(N,m)}+mG_z}{k_0}\right)
\begin{pmatrix}
\underline{\tilde{E}}_y\big|_{-N+m}^{N+m} \\
\underline{\tilde{E}}_x\big|_{-N+m}^{N+m} \\
\underline{\tilde{H}}_y\big|_{-N+m}^{N+m} \\
\underline{\tilde{H}}_x\big|_{-N+m}^{N+m}
\end{pmatrix}. \tag{25}
$$

As proven in Appendix A, the number of nontrivial pseudo-Fourier representations of a pseudo-Fourier eigenmode is $2N+1$. We can consider the corresponding $2N+1$ nontrivial vectors $[\underline{\tilde{E}}_y|_0^{2N}\ \underline{\tilde{E}}_x|_0^{2N}\ \underline{\tilde{H}}_y|_0^{2N}\ \underline{\tilde{H}}_x|_0^{2N}]^t$, $\ldots$, $[\underline{\tilde{E}}_y|_{-2N}^{0}\ \underline{\tilde{E}}_x|_{-2N}^{0}\ \underline{\tilde{H}}_y|_{-2N}^{0}\ \underline{\tilde{H}}_x|_{-2N}^{0}]^t$ as the eigenvectors of the following eigenvalue equation:

$$
\begin{bmatrix}
-j\underline{\underline{G}}_z\big|_{-N}^{N} & 0 & \underline{\underline{K}}_y\underline{\underline{\alpha}}\underline{\underline{K}}_x & \underline{\underline{\mu}}-\underline{\underline{K}}_y\underline{\underline{\alpha}}\underline{\underline{K}}_y \\
0 & -j\underline{\underline{G}}_z\big|_{-N}^{N} & -\underline{\underline{\mu}}+\underline{\underline{K}}_x\underline{\underline{\alpha}}\underline{\underline{K}}_x & -\underline{\underline{K}}_x\underline{\underline{\alpha}}\underline{\underline{K}}_y \\
\underline{\underline{K}}_y\underline{\underline{\beta}}\underline{\underline{K}}_x & \underline{\underline{\varepsilon}}-\underline{\underline{K}}_y\underline{\underline{\beta}}\underline{\underline{K}}_y & -j\underline{\underline{G}}_z\big|_{-N}^{N} & 0 \\
-\underline{\underline{\varepsilon}}+\underline{\underline{K}}_x\underline{\underline{\beta}}\underline{\underline{K}}_x & -\underline{\underline{K}}_x\underline{\underline{\beta}}\underline{\underline{K}}_y & 0 & -j\underline{\underline{G}}_z\big|_{-N}^{N}
\end{bmatrix}
\times\begin{pmatrix}
\underline{E}_y \\ \underline{E}_x \\ \underline{H}_y \\ \underline{H}_x
\end{pmatrix}
=\beta\begin{pmatrix}
\underline{E}_y \\ \underline{E}_x \\ \underline{H}_y \\ \underline{H}_x
\end{pmatrix}. \tag{26}
$$

Their own β eigenvalues are identified, respectively, as

$$-jk_0\beta = k_z^{(N,N)} + NG_z, \ldots, k_z^{(N,-N)} - NG_z. \tag{27}$$

These $2N+1$ nontrivial eigenvector–eigenvalue pairs are approximate pseudo-Fourier representations of a true pseudo-Fourier eigenmode with eigenvalue k_z.

On the other hand, the dimension of the matrix in Eq. (26) is $(8N+4)\times(8N+4)$. The number of nontrivial eigenvector–eigenvalue pairs of Eq. (26) is $8N+4$. Therefore just four different pseudo-Fourier eigenmodes can be identified in the scheme of Eq. (26) because $8N+4$ eigenpairs are classified into each homogeneous group composed of $2N+1$ eigenpairs. Physically, this means that only four pseudo-Fourier eigenmodes exist in the periodic extensions of dielectric slabs with $\hat{\varepsilon}(z)$ and $\hat{\mu}(z)$.

To correctly distinguish the four pseudo-Fourier eigenmodes among $8N+4$ eigenvector–eigenvalue pairs of Eq. (26), the wavenumbers in the first Brillouin zone must be extracted from each obtained eigenvalue. Explicitly the wavenumber in the first Brillouin zone, $\tilde{\beta}_{\text{1st Brill}}$, can be extracted by the following formula:

$$\tilde{\beta}_{\text{1st Brill}} = \beta - G_z[(\mathrm{Im}(\beta)+0.5G_z)\mathrm{mod}(G_z)], \tag{28}$$

where $\mathrm{Im}(\eta)$ indicates the imaginary part of a complex number η. If $m=(\mathrm{Im}(\beta)+0.5G_z)\mathrm{mod}(G_z)$ is satisfied, the first Brillouin zone wavenumber $\tilde{\beta}_{\text{1st Brill}}$ and its corresponding eigenvector $[\underline{E}_y\ \ \underline{E}_x\ \ \underline{H}_y\ \ \underline{H}_x]^t$ are identified, respectively, as $[\underline{\tilde{E}}_y|_{-N+m}^{N+m}\ \ \underline{\tilde{E}}_x|_{-N+m}^{N+m}\ \ \underline{\tilde{H}}_y|_{-N+m}^{N+m}\ \ \underline{\tilde{H}}_x|_{-N+m}^{N+m}]^t$ and $k_z^{(N,m)}$. It is reasonable to select the symmetric representation $(\underline{E}_g^{(N,0)}(z), \underline{H}_g^{(N,0)}(z))$ among $2m^*(N)+1$ pseudo-Fourier representations of a pseudo-Fourier eigenmode in class (ii) to construct the pseudo-Fourier eigenmode $(\underline{E}_g(z), \underline{H}_g(z))$. Here, for the convenience, the mode index is denoted by g instead of $\underline{k}$. Then the mode selection rule is simplified. We just select the individuals satisfying the following relation among the obtained $8N+4$ eigenvalues [see Eq. (28)]:

$$(\mathrm{Im}(\beta)+0.5G_z)\mathrm{mod}(G_z) = 0. \tag{29}$$

It is confirmed that the number of individuals satisfying that condition is exactly four. Conclusively we can easily identify four pseudo-Fourier eigenmodes with the method described above.

4. PSEUDO-FOURIER EIGENMODE EXTRACTION

To validate the theory described in Section 2, we present two illustrative examples. Figures 4(a) and 4(b) show a 4λ thickness dielectric slab with longitudinal continuous permittivity and permeability profiles, and a 4λ thickness dielectric slab with longitudinal discrete permittivity and

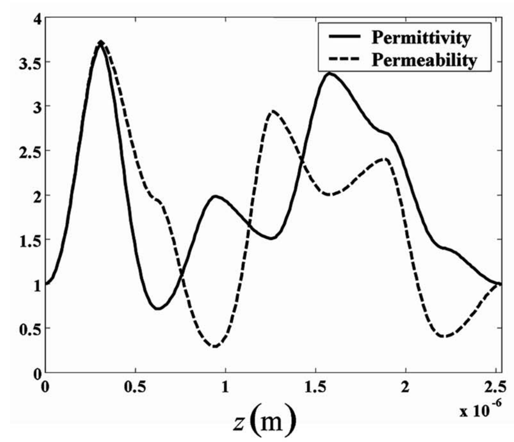

(a)

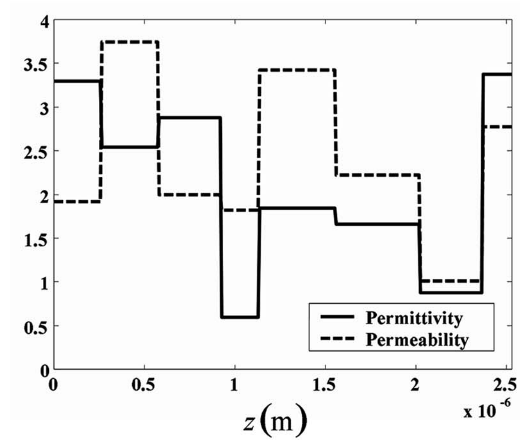

(b)

Fig. 4. Dielectric structure with thickness of 4λ and (a) longitudinal continuous permittivity and permeability profiles and (b) longitudinal discrete permittivity and permeability profiles.

permeability profiles, respectively. In this section, the pseudo-Fourier eigenmodes and eigenvalues of two comparative structures are extracted with the PFMA.

In the analysis, the plane wave, with incidence angle of $\pi/4$, azimuthal angle of $\pi/3$, polarization angle of $\pi/4$, and unit intensity, is taken as the external incident source. At first, the dielectric slab with continuous permittivity and permeability profiles shown in Fig. 4(a) is analyzed. Figure 5 shows the eigenvalue distributions that are obtained by solving the main eigenvalue Eq. (26) and folding the eigenvalues to the first Brillouin zone with use of Eqs. (27) and (28). In Fig. 5, the imaginary part of $jk_z^{(N,m)}$ scaled by k_0 is plotted. If $k_z^{(N,m)}$ is a pure real number, the corresponding eigenmode $(\underline{E}_k^{(N,m)}(z),\underline{H}_k^{(N,m)}(z))$ is referred to as a nonevanescent mode, while if the imaginary part of $k_z^{(N,m)}$ is nonzero, the corresponding eigenmode $(\underline{E}_k^{(N,m)}(z),\underline{H}_k^{(N,m)}(z))$ is referred to as an evanescent mode. Figure 5(a) shows the eigenvalue distribution when the number of harmonic components used in the pseudo-Fourier representation, $2N+1$, is 21. As indicated in Fig. 5(a), the convergence of the eigenvalue is not perceived due to the insufficient number of Fourier harmonic components. According to the classification rule of the pseudo-Fourier representations, all representations used in this case are included in class (iii). On the other hand, Fig. 5(b) illustrates the case in which a sufficient number of harmonic components ($2N+1=129$) are used in the field representation. As seen in

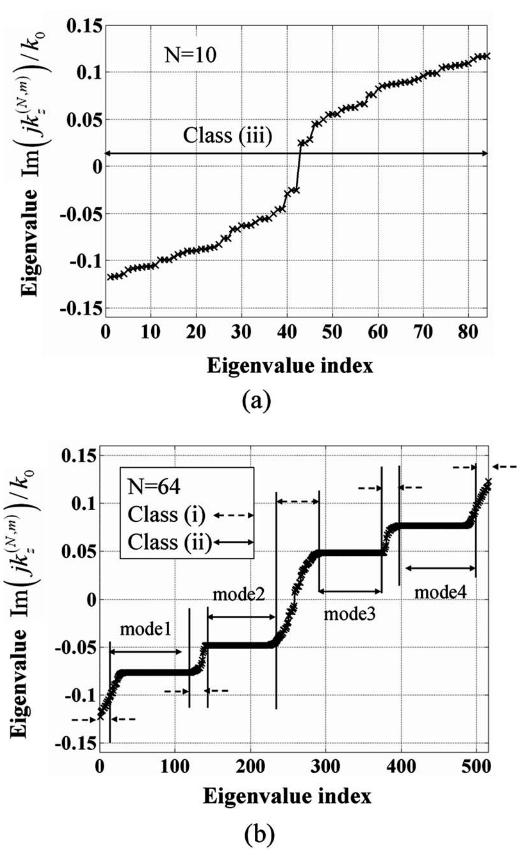

Fig. 5. Analyzed eigenvalue distributions in the first Brillouin zone of the dielectric slab with continuous permittivity and permeability profiles when (a) $N=10$ and (b) $N=64$.

Fig. 5(b), four flat portions appear in the eigenvalue distribution plot. It is noted that there exist unflat transition regions between adjacent flat intervals, i.e., nonconvergent eigenvalues. The Fourier representations corresponding to the flat portions belong to class (ii), but those corresponding to the nonconvergent eigenvalues are classified into class (i).

Among the convergent pseudo-Fourier representations, four symmetric representations, $(\underline{E}_g^{(N,0)}(z),\underline{H}_g^{(N,0)}(z))$, are selected for building the gth pseudo-Fourier eigenmode $(\underline{E}_g(z),\underline{H}_g(z))$ that can be extracted with the use of Eq. (29).

Considering the eigenvalue distribution in Fig. 5(b), we can understand that two pseudo-Fourier eigenmodes, $(\underline{E}_1(z),\underline{H}_1(z))$ and $(\underline{E}_2(z),\underline{H}_2(z))$, propagate backward along the z direction and are orthogonally polarized to each other. The other pseudo-Fourier eigenmodes, $(\underline{E}_3(z),\underline{H}_3(z))$ and $(\underline{E}_4(z),\underline{H}_4(z))$, are also orthogonally polarized to each other and propagate forward along the z direction. From the symmetry of the eigenvalue distribution, we can see that $(\underline{E}_1(z),\underline{H}_1(z))$ is the conjugate mode of $(\underline{E}_4(z),\underline{H}_4(z))$, and $(\underline{E}_2(z),\underline{H}_2(z))$ is the conjugate mode of $(\underline{E}_3(z),\underline{H}_3(z))$. Figure 6 illustrates the field distributions of the four extracted pseudo-Fourier eigenmodes inside the dielectric slab, $(\underline{E}_1(z),\underline{H}_1(z)),\ldots,(\underline{E}_4(z),\underline{H}_4(z))$. In the case of the continuous structure, four scaled eigenvalues (scaled by $-jk_0$ for convenience) are obtained, respectively, as $jk_z^{(1)}/k_0=-0.0767j$, $jk_z^{(2)}/k_0=-0.0483j$, $jk_z^{(3)}/k_0=+0.0483j$, and $jk_z^{(4)}/k_0=+0.0767j$. Thus all extracted pseudo-Fourier eigenmodes are nonevanescent modes.

However, in the second example of the dielectric slab with discrete permittivity and permeability profiles shown in Fig. 4(b), all four extracted pseudo-Fourier eigenmodes are evanescent modes. Especially it is noted that the analytic Fourier representations of the discrete permittivity and permeability profiles provided in Appendix B should be used in the calculation to achieve high accuracy.

Figure 7(a) shows the eigenvalue distribution for the discrete case when the number of harmonic components used in the pseudo-Fourier representation is insufficient ($2N+1=21$), while Fig. 7(b) shows the convergent eigenvalue distribution with use of sufficient harmonic components ($2N+1=129$). Figure 8 illustrates the field distributions of the four extracted pseudo-Fourier eigenmodes inside the dielectric slab, $(\underline{E}_1(z),\underline{H}_1(z)),\ldots,(\underline{E}_4(z),\underline{H}_4(z))$. In this case, the extracted eigenvalues are obtained, respectively, as $jk_z^{(1)}/k_0=-0.0205$, $jk_z^{(2)}/k_0=-0.0163$, $jk_z^{(3)}/k_0=+0.0163$, and $jk_z^{(4)}/k_0=+0.0205$. Thus all extracted pseudo-Fourier eigenmodes are evanescent modes. This point is definitely indicated in the eigenvalue distribution illustrated in Fig. 7(b). When a sufficient number of harmonic components ($2N+1=121$) are used in the field representation, as seen in Fig. 7(b), a wide flat portion appears near the center axis since all eigenvalues are pure imaginary numbers. Inspecting the distribution of $\mathrm{Re}(jk_z^{(N,m)})/k_0$, we can see that the eigenvalues in the center flat portion are pure real numbers. That means that the flat portion includes four independent evanescent eigenmodes. It is noted that the evanescent modes $(\underline{E}_1(z),\underline{H}_1(z))$ and $(\underline{E}_2(z),\underline{H}_2(z))$ are exponentially decreas-

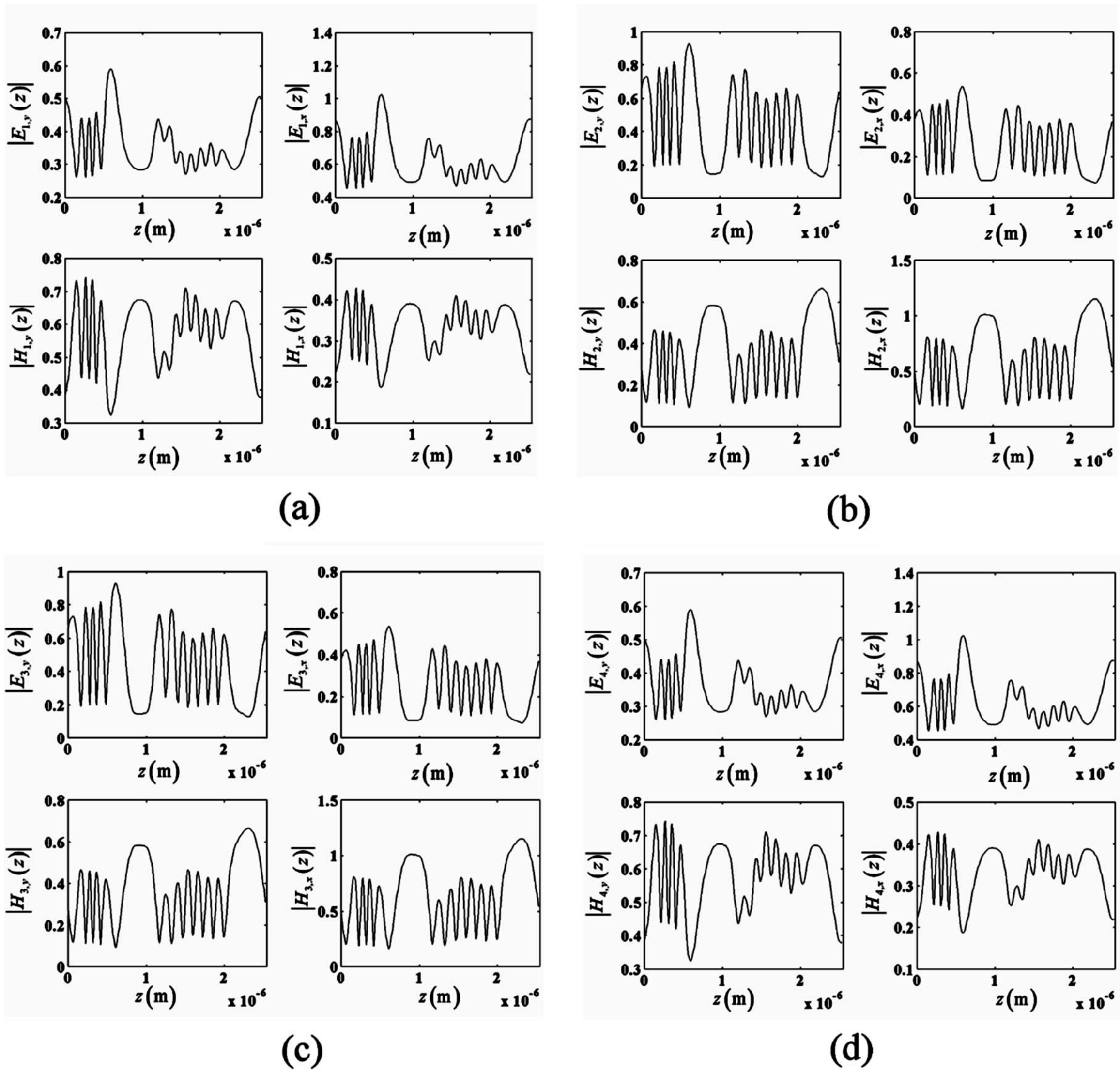

Fig. 6. Extracted pseudo-Fourier eigenmodes of the dielectric slab with continuous permittivity and permittivity profiles: (a) $(\underline{E}_1(z),\underline{H}_1(z))$ with $jk_z^{(1)}/k_0=-0.0767j$, (b) $(\underline{E}_2(z),\underline{H}_2(z))$ with $jk_z^{(2)}/k_0=-0.0483j$, (c) $(\underline{E}_3(z),\underline{H}_3(z))$ with $jk_z^{(3)}/k_0=+0.0483j$, (d) $(\underline{E}_4(z),\underline{H}_4(z))$ with $jk_z^{(4)}/k_0=+0.0767j$.

ing along the z direction, but the evanescent modes $(\underline{E}_3(z),\underline{H}_3(z))$ and $(\underline{E}_4(z),\underline{H}_4(z))$ seem to be exponentially increasing along the z direction. The exponentially increasing evanescent mode may be somewhat unphysical, but these increasing evanescent modes play a role in representing the real evanescent field near the backside boundary $(z=d)$ of the finite structure.

5. BOUNDARY CONDITION AND TOTAL FIELD DISTRIBUTION

In Sections 3 and 4, the four pseudo-Fourier eigenmodes are identified for the periodic extension of a unit slab structure with finite thickness and longitudinal arbitrary permittivity and permeability profiles. In this section, on the basis of the theoretical analysis on the pseudo-Fourier eigenmodes, the calculation of the total electromagnetic field distribution inside finite dielectric slabs is addressed. For the validity of the proposed PFMA method, the numerical results of the PFMA are compared with those of the conventional RCWA and S-matrix method.

The main principle is that the total electromagnetic field distribution inside a dielectric slab can be represented by a linear superposition of extracted pseudo-Fourier eigenmodes with appropriate coupling constants to satisfy given boundary conditions. Thus the total electric field distribution $\underline{E}$ and magnetic field distribution $\underline{H}$ are expressed, respectively, as

$$\underline{E}=\sum_{g=1}^{4}C_g\underline{E}_g(z)=\exp[j(k_xx+k_yy)]\sum_{g=1}^{4}C_g\left[\sum_{p=-N}^{N}(\tilde{E}_{x,p}^{(g)}\underline{x}+\tilde{E}_{y,p}^{(g)}\underline{y}+\tilde{E}_{z,p}^{(g)}\underline{z})\exp(jpG_zz)\right]\exp(jk_{z,g}z), \tag{30a}$$

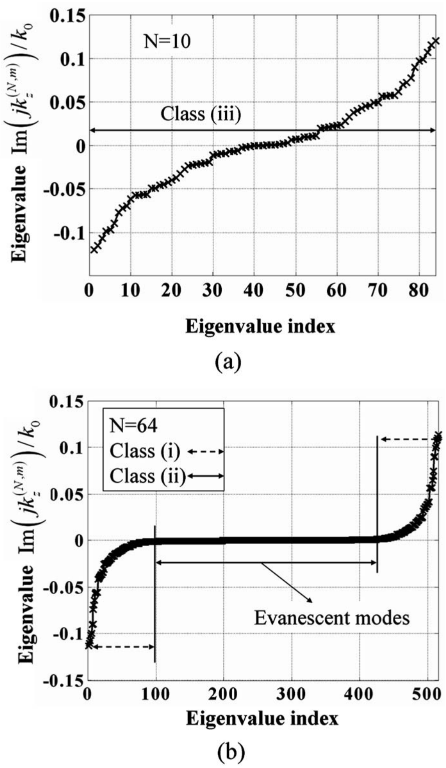

Fig. 7. Analyzed eigenvalue distributions in the first Brillouin zone of the dielectric slab with discrete permittivity and permeability profiles when (a) $N=10$ and (b) $N=64$.

$$\underline{H}=\sum_{g=1}^{4} C_g \underline{H}_g(z)=\exp[j(k_x x+k_y y)]j\sqrt{\frac{\varepsilon_0}{\mu_0}}\sum_{g=1}^{4} C_g\left[\sum_{p=-N}^{N}(\tilde{H}_{x,p}^{(g)}\underline{x}+\tilde{H}_{y,p}^{(g)}\underline{y}+\tilde{H}_{z,p}^{(g)}\underline{z})\exp(jpG_z z)\right]\exp(jk_{z,g}z), \tag{30b}$$

where C_g is the coupling coefficient. The four coupling coefficients C_1, C_2, C_3, and C_4 must be determined to satisfy the boundary conditions specified at $z=z_-$ and $z=z_+$ ($z_- < z_+$). In fact, the field expressions of Eqs. (30a) and (30b) imply a general solution of the Maxwell Eqs. (30a) and (30b) inside a periodic extension of a unit permittivity profile. This means that two boundaries, $z=z_-$ and $z=z_+$, of the finite dielectric structure can be placed at any two positions inside the periodic extension shown in Fig. 2. The field expressions of Eqs. (30a) and (30b) can be exact total field distributions in the dielectric slab confined by the two boundaries $z=z_-$ and $z=z_+$. The proper determination of the four coupling coefficients is only required to satisfy the boundary conditions at the two boundaries. In the cases of the finite dielectric slab shown in Fig. 1, the first and the second boundaries are selected as $z_-=0$ and $z_+=d$, respectively,

The boundary conditions are described as follows. At $z=0$, the transverse electric and magnetic fields must be continuous. These conditions read as

$$u_y+R_y=\sum_{g=1}^{4} C_g\left(\sum_{p=-N}^{N}\tilde{E}_{y,p}^{(g)}\right), \tag{31a}$$

$$u_x+R_x=\sum_{g=1}^{4} C_g\left(\sum_{p=-N}^{N}\tilde{E}_{x,p}^{(g)}\right), \tag{31b}$$

$$(k_{\mathrm{I},z}u_x-k_x u_z)/k_0+(-k_{\mathrm{I},z}R_x-k_x R_z)/k_0=j\sum_{g=1}^{4} C_g\left(\sum_{p=-N}^{N}\tilde{H}_{y,p}^{(g)}\right), \tag{31c}$$

$$(k_y u_z-k_{\mathrm{I},z}u_y)/k_0+(k_y R_z+k_{\mathrm{I},z}R_y)/k_0=j\sum_{g=1}^{4} C_g\left(\sum_{p=-N}^{N}\tilde{H}_{x,p}^{(g)}\right). \tag{31d}$$

Using the aid of the transverse condition of the plane wave

$$k_x R_x+k_y R_y-k_{\mathrm{I},z}R_z=0, \tag{31e}$$

Eqs. (31a)–(31d) are arranged in the following matrix form:

$$\begin{pmatrix} u_y \\ u_x \\ (k_{\mathrm{I},z}u_x-k_x u_z)/k_0 \\ (k_y u_z-k_{\mathrm{I},z}u_y)/k_0 \end{pmatrix}+\begin{bmatrix} 1 & 0 \\ 0 & 1 \\ -\dfrac{k_x k_y}{k_0 k_{\mathrm{I},z}} & -\dfrac{(k_{\mathrm{I},z}^2+k_x^2)}{k_0 k_{\mathrm{I},z}} \\ \dfrac{(k_y^2+k_{\mathrm{I},z}^2)}{k_0 k_{\mathrm{I},z}} & \dfrac{k_y k_x}{k_0 k_{\mathrm{I},z}} \end{bmatrix}\begin{pmatrix} R_y \\ R_x \end{pmatrix}$$
$$=\begin{bmatrix} \sum_{p=-N}^{N}\tilde{E}_{y,p}^{(1)} & \sum_{p=-N}^{N}\tilde{E}_{y,p}^{(2)} & \sum_{p=-N}^{N}\tilde{E}_{y,p}^{(3)} & \sum_{p=-N}^{N}\tilde{E}_{y,p}^{(4)} \\ \sum_{p=-N}^{N}\tilde{E}_{x,p}^{(1)} & \sum_{p=-N}^{N}\tilde{E}_{x,p}^{(2)} & \sum_{p=-N}^{N}\tilde{E}_{x,p}^{(3)} & \sum_{p=-N}^{N}\tilde{E}_{x,p}^{(4)} \\ j\sum_{p=-N}^{N}\tilde{H}_{y,p}^{(1)} & j\sum_{p=-N}^{N}\tilde{H}_{y,p}^{(2)} & j\sum_{p=-N}^{N}\tilde{H}_{y,p}^{(3)} & j\sum_{p=-N}^{N}\tilde{H}_{y,p}^{(4)} \\ j\sum_{p=-N}^{N}\tilde{H}_{x,p}^{(1)} & j\sum_{p=-N}^{N}\tilde{H}_{x,p}^{(2)} & j\sum_{p=-N}^{N}\tilde{H}_{x,p}^{(3)} & j\sum_{p=-N}^{N}\tilde{H}_{x,p}^{(4)} \end{bmatrix}\times\begin{pmatrix} C_1 \\ C_2 \\ C_3 \\ C_4 \end{pmatrix}. \tag{32}$$

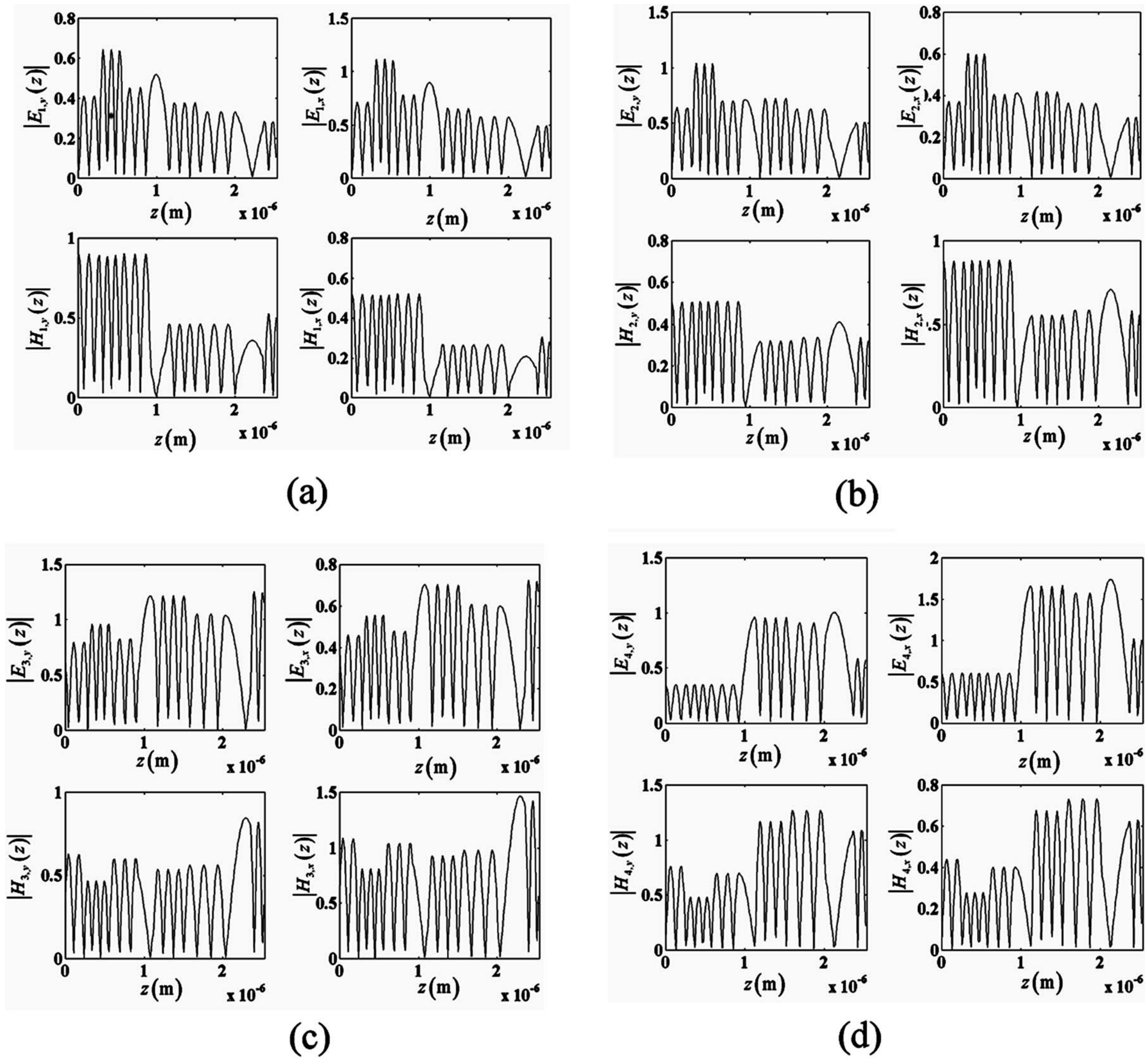

Fig. 8. Extracted pseudo-Fourier eigenmodes of the dielectric slab with discrete permittivity and permeability profiles: (a) $(\underline{E}_1(z),\underline{H}_1(z))$ with $jk_z^{(1)}/k_0=-0.0205$, (b) $(\underline{E}_2(z),\underline{H}_2(z))$ with $jk_z^{(2)}/k_0=-0.0163$, (c) $(\underline{E}_3(z),\underline{H}_3(z))$ with $jk_z^{(3)}/k_0=0.0163$, (d) $(\underline{E}_4(z),\underline{H}_4(z))$ with $jk_z^{(4)}/k_0=+0.0205$.

Next, at $z=d$, the continuation conditions of the transverse electric and magnetic fields read as

$$T_y=\sum_{g=1}^{4}C_g\left(\sum_{p=-N}^{N}\tilde{E}_{y,p}^{(g)}\exp(j(k_{z,g}+pG_z)d)\right), \tag{33a}$$

$$T_x=\sum_{g=1}^{4}C_g\left(\sum_{p=-N}^{N}\tilde{E}_{x,p}^{(g)}\exp(j(k_{z,g}+pG_z)d)\right), \tag{33b}$$

$$(k_{\mathrm{II},z}T_x-k_xT_z)/k_0=j\sum_{g=1}^{4}C_g\left(\sum_{p=-N}^{N}\tilde{H}_{y,p}^{(g)}\exp(j(k_{z,g}+pG_z)d)\right), \tag{33c}$$

$$(k_yT_z-k_{\mathrm{II},z}T_y)/k_0=j\sum_{g=1}^{4}C_g\left(\sum_{p=-N}^{N}\tilde{H}_{x,p}^{(g)}\exp(j(k_{z,g}+pG_z)d)\right). \tag{33d}$$

Using the transverse condition of the plane wave

$$k_xT_x+k_yT_y+k_{\mathrm{II},z}T_z=0, \tag{33e}$$

Eqs. (33a)–(33d) are arranged in the following matrix form:

$$\begin{bmatrix} \mathrm{I} & 0 \\ 0 & \mathrm{I} \\ \dfrac{k_y k_x}{k_0 k_{\mathrm{II},z}} & \dfrac{(k_{\mathrm{II},z}^2 + k_x^2)}{k_0 k_{\mathrm{II},z}} \\ -\dfrac{(k_y^2 + k_{\mathrm{II},z}^2)}{k_0 k_{\mathrm{II},z}} & -\dfrac{k_y k_x}{k_0 k_{\mathrm{II},z}} \end{bmatrix} \begin{pmatrix} T_y \\ T_x \end{pmatrix}$$

$$= \begin{bmatrix} \sum_{p=-N}^{N} \tilde{E}_{y,p}^{(1)} \exp(j(k_{z,1} + pG_z)d) & \sum_{p=-N}^{N} \tilde{E}_{y,p}^{(2)} \exp(j(k_{z,2} + pG_z)d) & \sum_{p=-N}^{N} \tilde{E}_{y,p}^{(3)} \exp(j(k_{z,3} + pG_z)d) & \sum_{p=-N}^{N} \tilde{E}_{y,p}^{(4)} \exp(j(k_{z,4} + pG_z)d) \\ \sum_{p=-N}^{N} \tilde{E}_{x,p}^{(1)} \exp(j(k_{z,1} + pG_z)d) & \sum_{p=-N}^{N} \tilde{E}_{x,p}^{(2)} \exp(j(k_{z,2} + pG_z)d) & \sum_{p=-N}^{N} \tilde{E}_{x,p}^{(3)} \exp(j(k_{z,3} + pG_z)d) & \sum_{p=-N}^{N} \tilde{E}_{x,p}^{(4)} \exp(j(k_{z,4} + pG_z)d) \\ j\sum_{p=-N}^{N} \tilde{H}_{y,p}^{(1)} \exp(j(k_{z,1} + pG_z)d) & j\sum_{p=-N}^{N} \tilde{H}_{y,p}^{(2)} \exp(j(k_{z,2} + pG_z)d) & j\sum_{p=-N}^{N} \tilde{H}_{y,p}^{(3)} \exp(j(k_{z,3} + pG_z)d) & j\sum_{p=-N}^{N} \tilde{H}_{y,p}^{(4)} \exp(j(k_{z,4} + pG_z)d) \\ j\sum_{p=-N}^{N} \tilde{H}_{x,p}^{(1)} \exp(j(k_{z,1} + pG_z)d) & j\sum_{p=-N}^{N} \tilde{H}_{x,p}^{(2)} \exp(j(k_{z,2} + pG_z)d) & j\sum_{p=-N}^{N} \tilde{H}_{x,p}^{(3)} \exp(j(k_{z,3} + pG_z)d) & j\sum_{p=-N}^{N} \tilde{H}_{x,p}^{(4)} \exp(j(k_{z,4} + pG_z)d) \end{bmatrix} \begin{pmatrix} C_1 \\ C_2 \\ C_3 \\ C_4 \end{pmatrix}. \quad (34)$$

The four coupling coefficients C_1, C_2, C_3, and C_4 and the reflection and transmission coefficients R_x, R_y, T_x, and T_y can be obtained from Eqs. (32) and (34). By this manner, the total field distributions inside the dielectric slabs in Figs. 4(a) and 4(b) are calculated. These are compared with those of the RCWA with the S-matrix.

Total electric field distributions in the dielectric slab with continuous permittivity and permeability profiles calculated by the PFMA are illustrated in Fig. 9. The y-directional electric field component $E_y(z)$ and the x-directional electric field component $E_x(z)$ are presented in Figs. 9(a) and 9(b), respectively. For the RCWA with the S-matrix method, the continuous profiles of the permittivity and permeability are quantized to the multilevel staircase structure as shown in Fig. 10. In Fig. 11, the total field distributions obtained by the RCWA with the S-matrix method are presented. Comparing the field distributions in Figs. 9 and 11, we can see that the numerical results obtained by the proposed PFMA method show an excellent agreement with those of the conventional RCWA with the S-matrix method.

Total electric field distributions in the dielectric slab with discrete permittivity and permeability profiles calculated by the PFMA are illustrated in Fig. 12. The y-directional electric field component $E_y(z)$ and the x-directional electric field component $E_x(z)$ are presented in Figs. 12(a) and 12(b), respectively. In Fig. 13, the total field distributions obtained by the RCWA with the S-matrix method are presented for a comparison. Comparing the field distributions in Figs. 12 and 13, we can see that the proposed PFMA method shows an excellent agreement with the conventional RCWA with the S-matrix method in the case of discrete profiles.

6. CONCLUSION

In this paper, a PFMA method for analyzing finite-sized dielectric slabs with arbitrary longitudinal permittivity and permeability profiles without the staircase approximation was proposed. In the PFMA, the internal pseudo-Fourier eigenmodes are extracted with specific eigenvalues. The eigenvalues can be obtained by the eigenvalue distribution analysis using the asymmetrically truncated Fourier field representation. It was shown that the total field distribution inside the finite-sized dielectric slab excited by an external plane wave can be precisely calculated by the linear superposition of four pseudo-Fourier

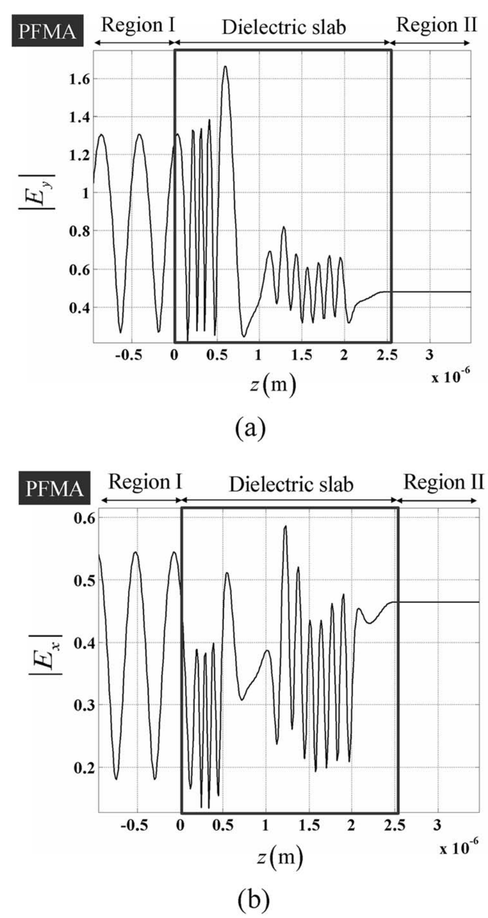

Fig. 9. Total electric field distributions in the dielectric slab with continuous permittivity and permeability profiles (a) E_y (z) and (b) E_x (z) obtained by the PFMA.

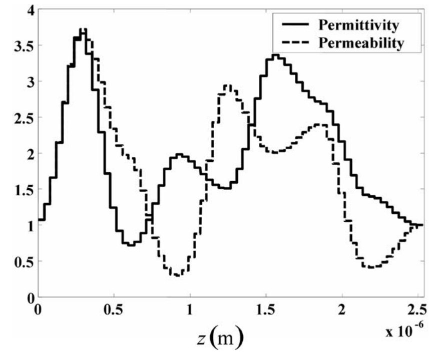

Fig. 10. Staircase approximation of the continuous permittivity and permeability profiles in the dielectric slab obtained by the RCWA with the S-matrix method.

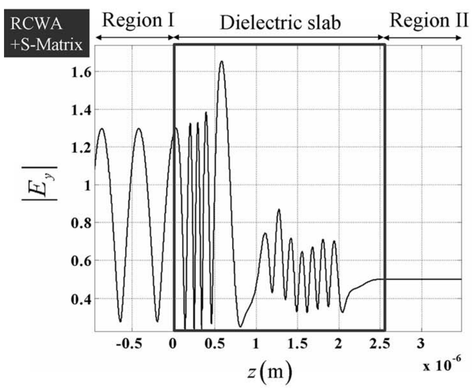

(a)

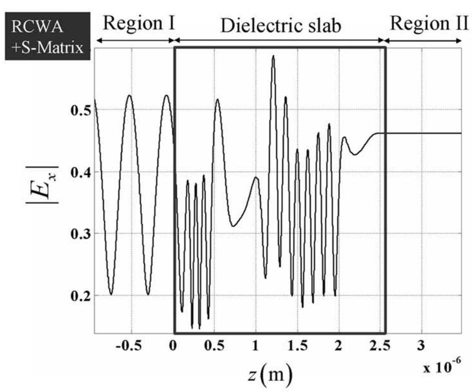

(b)

Fig. 11. Total electric field distributions in the dielectric slab with continuous permittivity and permeability profiles (a) $E_y(z)$ and (b) $E_x(z)$ obtained by the S-matrix method and the (one-dimensional version) RCWA.

eigenmodes with appropriate coupling coefficients satisfying the boundary conditions. The validity of the PFMA is proved by the excellent agreement of the PFMA with the conventional RCWA with the S-matrix method. The mathematical techniques of dealing with longitudinal permittivity and permeability profiles and extracting pseudo-Fourier eigenmodes in the PFMA are general, so they can be directly extended to analyze three-dimensional structures. The pseudo-Fourier mode-based representation of the internal electromagnetic field is more precise and better in convergence than the simple Fourier representation.[11,12] The PFMA method is a complete modal analysis method for finite-sized dielectric slabs with arbitrary three-dimensional permittivity and permeability profiles.

APPENDIX A

Here it is proved that the number of the nontrivial pseudo-Fourier representations of a pseudo-Fourier eigenmode is $2N+1$. For simplicity, only the permittivity modulation is taken into account. A pseudo-Fourier mode of the periodic series of the dielectric slab is substituted into Maxwell's equations as

$$\nabla \times [\exp(j(\underline{k} \cdot \underline{r}))\underline{E}] = j\omega\mu_0[\exp(j(\underline{k} \cdot \underline{r}))\underline{H}], \qquad \text{(A1)}$$

$$\nabla \times [\exp(j(\underline{k} \cdot \underline{r}))\underline{H}] = -j\omega\varepsilon_0\varepsilon(z)[\exp(j(\underline{k} \cdot \underline{r}))\underline{E}]. \qquad \text{(A2)}$$

Let the dc terms of the permittivity profile, the electric eigenmode, and the magnetic eigenmode be defined as follows:

$$\tilde{\varepsilon}_0 = \int_0^d \varepsilon(z)\mathrm{d}z, \qquad \text{(A3)}$$

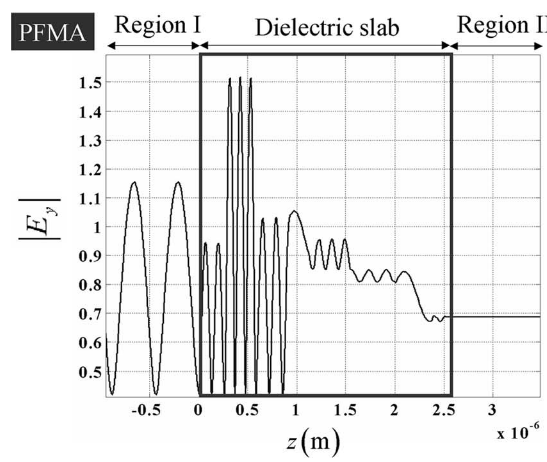

(a)

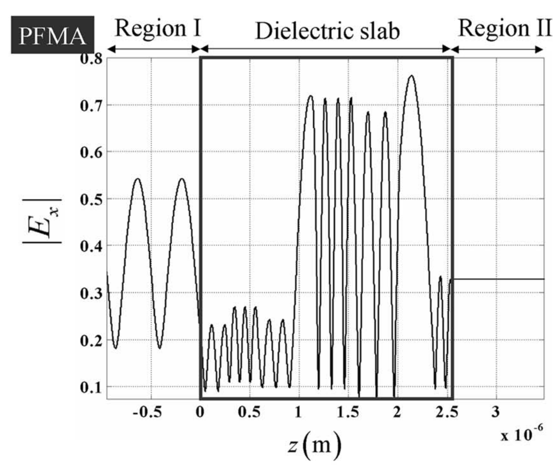

(b)

Fig. 12. Total electric field distributions in the dielectric slab with discrete permittivity and permeability profiles (a) $E_y(z)$ and (b) $E_x(z)$ obtained by the PFMA.

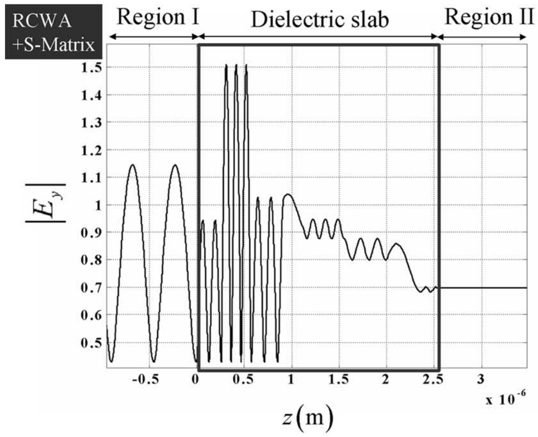

(a)

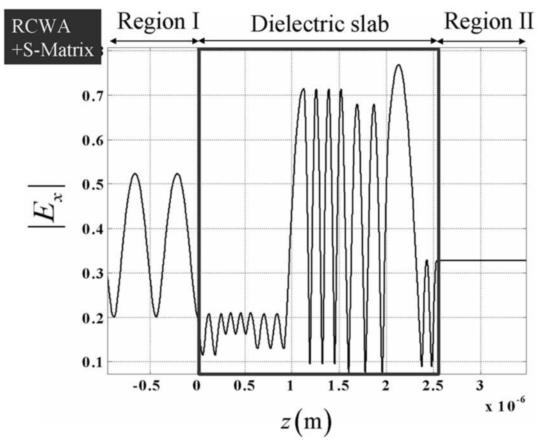

(b)

Fig. 13. Total electric field distributions in the dielectric slab with discrete permittivity and permeability profiles (a) $E_y(z)$ and (b) $E_x(z)$ obtained by the S-matrix method and the (one-dimensional version) RCWA.

$$\underline{\tilde{E}}_0 = \int_0^d \underline{E}(z)\mathrm{d}z, \tag{A4}$$

$$\underline{\tilde{H}}_0 = \int_0^d \underline{H}(z)\mathrm{d}z. \tag{A5}$$

Next, using Eqs. (A3)–(A5), let the following manipulation of the Maxwell Eqs. (A1) and (A2) be performed:

$$\nabla \times [\exp(j(\underline{k}\cdot\underline{r}))(\underline{E}-\underline{\tilde{E}}_0+\underline{\tilde{E}}_0)] = j\omega\mu_0[\exp(j(\underline{k}\cdot\underline{r}))(\underline{H}-\underline{\tilde{H}}_0+\underline{\tilde{H}}_0)], \tag{A6}$$

$$\nabla \times [\exp(j(\underline{k}\cdot\underline{r}))(\underline{H}-\underline{\tilde{H}}_0+\underline{\tilde{H}}_0)] = -j\omega\varepsilon_0[\varepsilon(z)-\tilde{\varepsilon}_0+\tilde{\varepsilon}_0][\exp(j(\underline{k}\cdot\underline{r}))(\underline{E}-\underline{\tilde{E}}_0+\underline{\tilde{E}}_0)]. \tag{A7}$$

After further manipulation, we get

$$\nabla \times [\exp(j(\underline{k}\cdot\underline{r}))(\underline{E}-\underline{\tilde{E}}_0)] + \nabla \times [\exp(j(\underline{k}\cdot\underline{r}))\underline{\tilde{E}}_0] = j\omega\mu_0[\exp(j(\underline{k}\cdot\underline{r}))(\underline{H}-\underline{\tilde{H}}_0)] + j\omega\mu_0[\exp(j(\underline{k}\cdot\underline{r}))\underline{\tilde{H}}_0], \tag{A8}$$

$$\nabla \times [\exp(j(\underline{k}\cdot\underline{r}))(\underline{H}-\underline{\tilde{H}}_0)] + \nabla \times [\exp(j(\underline{k}\cdot\underline{r}))\underline{\tilde{H}}_0] = -j\omega\varepsilon_0\tilde{\varepsilon}_0[\exp(j(\underline{k}\cdot\underline{r}))(\underline{E}-\underline{\tilde{E}}_0)] - j\omega\varepsilon_0\tilde{\varepsilon}_0[\exp(j(\underline{k}\cdot\underline{r}))\underline{E}] - j\omega\varepsilon_0(\varepsilon(z)-\tilde{\varepsilon}_0)[\exp(j(\underline{k}\cdot\underline{r}))\underline{E}]. \tag{A9}$$

We can separate Eqs. (A8) and (A9) into two parts as follows:

(i) $$\nabla \times [\exp(j(\underline{k}\cdot\underline{r}))\underline{\tilde{E}}_0] = j\omega\mu_0[\exp(j(\underline{k}\cdot\underline{r}))\underline{\tilde{H}}_0], \tag{A10}$$

$$\nabla \times [\exp(j(\underline{k}\cdot\underline{r}))\underline{\tilde{H}}_0] = -j\omega\varepsilon_0\tilde{\varepsilon}_0[\exp(j(\underline{k}\cdot\underline{r}))\underline{E}], \tag{A11}$$

(ii) $$\nabla \times [\exp(j(\underline{k}\cdot\underline{r}))(\underline{E}-\underline{\tilde{E}}_0)] = j\omega\mu_0[\exp(j(\underline{k}\cdot\underline{r}))(\underline{H}-\underline{\tilde{H}}_0)], \tag{A12}$$

$$\nabla \times [\exp(j(\underline{k}\cdot\underline{r}))(\underline{H}-\underline{\tilde{H}}_0)] = -j\omega\varepsilon_0\tilde{\varepsilon}_0[\exp(j(\underline{k}\cdot\underline{r}))(\underline{E}-\underline{\tilde{E}}_0)] - j\omega\varepsilon_0(\varepsilon(z)-\tilde{\varepsilon}_0)[\exp(j(\underline{k}\cdot\underline{r}))\underline{E}]. \tag{A13}$$

Part (i) must have a nontrivial solution. That means that the representation of the electromagnetic field inside the slab must include a dc spectrum that is not zero. Thus, the total number of Fourier representations of the true eigenmode is $2N+1$ when the number of plane-wave components is $2N+1$. Therefore, approximate representations for $\exp(j(\underline{k}\cdot\underline{r}))=\exp(j(k_{x,0}x+k_{y,0}y+k_{z,0}z))$ read as follows:

$$\underline{E}^{(N)}(z) = \sum_{p=0}^{2N}(\tilde{E}_{x,p}\underline{x}+\tilde{E}_{y,p}\underline{y}+\tilde{E}_{z,p}\underline{z})\exp(jpG_z z),$$

$$k_z = k_{z,0} + \Delta k^{(N)}, \tag{A14}$$

$$\underline{E}^{(N-1)}(z) = \sum_{p=-1}^{2N-1}(\tilde{E}_{x,p}\underline{x}+\tilde{E}_{y,p}\underline{y}+\tilde{E}_{z,p}\underline{z})\exp(jpG_z z),$$

$$k_z = k_{z,0} + \Delta k^{(N-1)}, \tag{A15}$$

…

$$\underline{E}^{-(N-1)}(z) = \sum_{p=-(2N-1)}^{1}(\tilde{E}_{x,p}\underline{x}+\tilde{E}_{y,p}\underline{y}+\tilde{E}_{z,p}\underline{z})\exp(jpG_z z),$$

$$k_z = k_{z,0} + \Delta k^{-(N-1)}, \tag{A16}$$

$$\underline{E}^{-N}(z) = \sum_{p=-2N}^{0}(\tilde{E}_{x,p}\underline{x}+\tilde{E}_{y,p}\underline{y}+\tilde{E}_{z,p}\underline{z})\exp(jpG_z z),$$

$$k_z = k_{z,0} + \Delta k^{-N}. \tag{A17}$$

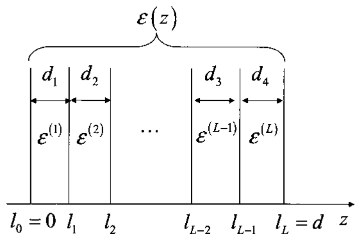

Fig. 14. Discrete permittivity profile with L homogeneous layers.

APPENDIX B

The Fourier coefficients of a discrete permittivity (permeability) profile can be analytically obtained as follows. The discrete permittivity profile with L homogeneous layers is described in Fig. 14. In each section, the thickness and the permittivity value in the pth section are denoted by d_p and $\varepsilon^{(p)}$, respectively. The boundaries between the adjacent pth layer and the $(p+1)$th layer are indicated by l_p and l_{p+1} as shown in Fig. 14. Then it is easily proven that the periodic extension $\tilde{\varepsilon}(z)$ of the permittivity profile $\varepsilon(z)$ is represented by the Fourier expansion

$$\tilde{\varepsilon}(z)=\sum_{k=-2N}^{k=2N}\tilde{\varepsilon}_k \exp\left(j\frac{2\pi k}{d}z\right), \tag{B1}$$

where the Fourier coefficient $\tilde{\varepsilon}_k$ is given by

$$\tilde{\varepsilon}_k=\sum_{p=1}^{L}\frac{\tilde{\varepsilon}_p d_p}{d}\,\mathrm{sinc}\left(\frac{d_p k}{d}\right)\exp\left(-j\frac{\pi k}{d}(l_{p-1}+l_p)\right). \tag{B2}$$

Contact information for B. Lee, the corresponding author, is as follows: e-mail, byoungho@snu.ac.kr; phone, 82-2-880-7245; fax, 82-2-873-9953.

REFERENCES

1. D. F. Felbacq and F. Zolla, "Scattering theory of photonic crystals," in *Introduction to Complex Mediums for Optics and Electromagnetics*, Vol. PM123 of the SPIE Press Monographs, W. S. Weiglhofer and A. Lakhtakia, eds. (SPIE Press, 2003).
2. M. G. Moharam and T. K. Gaylord, "Rigorous coupled-wave analysis of planar-grating diffraction," J. Opt. Soc. Am. **71**, 811–818 (1981).
3. P. Lalanne and G. M. Morris, "Highly improved convergence of the coupled-wave method for TM polarization," J. Opt. Soc. Am. A **13**, 779–784 (1996).
4. P. Lalanne, "Improved formulation of the coupled-wave method for two-dimensional gratings," J. Opt. Soc. Am. A **14**, 1592–1598 (1997).
5. L. Li, "Fourier modal method for crossed anisotropic gratings with arbitrary permittivity and permeability tensors," J. Opt. A, Pure Appl. Opt. **5**, 345–355 (2003).
6. L. Li, "Formulation and comparison of two recursive matrix algorithms for modeling layered diffraction gratings," J. Opt. Soc. Am. A **13**, 1024–1035 (1996).
7. M. Neviere and E. Popov, *Light Propagation in Periodic Media: Differential Theory and Design* (Marcel Dekker, 2002).
8. Y. Jeong and B. Lee, "Nonlinear property analysis of long-period fiber gratings using discretized coupled-mode theory," IEEE J. Quantum Electron. **35**, 1284–1292 (1999).
9. E. Popov, M. Neviere, B. Gralak, and G. Tayeb, "Staircase approximation validity for arbitrary-shaped gratings," J. Opt. Soc. Am. A **19**, 33–42 (2002).
10. E. Popov and M. Neviére, "Differential theory for diffraction gratings: a new formulation for TM polarization with rapid convergence," Opt. Lett. **25**, 598–600 (2000).
11. K. Sakoda, "Optical transmittance of a two-dimensional triangular photonic lattice," Phys. Rev. B **51**, 4672–4675 (1995).
12. K. Sakoda, *Optical Properties of Photonic Crystals* (Springer, 2001).
13. J. D. Joannopoulos, R. D. Meade, and J. N. Winn, *Photonic Crystal: Molding the Flow of Light* (Princeton U. Press, 1995).
14. L. Li, "Use of Fourier series in the analysis of discontinuous periodic structures," J. Opt. Soc. Am. A **13**, 1870–1876 (1996).